Universality of probability density functions in turbulent channel flow

Surya P. G. Dinavahi[a)]
AS&M, Inc., Hampton, Virginia 23666

Kenneth S. Breuer
Department of Aeronautics and Astronautics, Massachusetts Institute of Technology, Cambridge, Massachusetts 02139

Lawrence Sirovich
Center for Fluid Mechanics, Brown University, Providence, Rhode Island 02912

(Received 5 August 1993; accepted 30 January 1995)

Probability density functions (PDFs) of the fluctuating velocity components, as well as their first and second derivatives, are calculated using data from the direct numerical simulations (DNS) of fully developed turbulent channel flow. It is observed that, beyond the buffer region, the PDF of each of these quantities (except for $u_{,y}$), is independent of the distance from the channel wall. It is further observed that, beyond the buffer region, the PDFs are also independent of Reynolds number. Similar behavior is observed for the PDFs of the second derivatives. The pseudodissipation rate of kinetic energy exhibits lognormal behavior. © *1995 American Institute of Physics.*

I. INTRODUCTION

It has long been known that the probability density functions (PDFs) of the velocity fluctuations in isotropic turbulence are nearly Gaussian, whereas those of the velocity derivatives deviate significantly from Gaussian. This behavior was observed in grid generated turbulence experiments[1,2] and also in the DNS of isotropic turbulence.[3] The first derivatives of the velocities are observed to have exponential tails, Narasimha.[4] However, the "pseudodissipation" rate of kinetic energy, which is the sum of squares of the velocity derivatives, is known to exhibit lognormal behavior (e.g., Ref. 2).

The fact that, even though the PDFs of the velocities are close to Gaussian, the derivative PDFs have exponential tails, implies that the behavior of the small-scale structures is not influenced significantly by the presence of the larger-scale structures. The presence of exponential tails in the PDFs of the derivatives implies greater intermittency in the small-scale structures. Studying the PDFs of velocity and its derivatives should help in understanding the physics underlying the various processes in turbulence, and also in developing turbulence models.

The independence of PDFs in the wall normal direction (at one Reynolds number), in the Rayleigh–Bénard convection problem, was shown by Balachandar and Sirovich.[5] Preliminary study of the channel flow by Dinavahi[6] shows that the PDFs of velocities and their derivatives are independent of the wall normal distance. The aim of the present work is to observe the nature of the PDFs of the velocity, their derivatives, and the energy dissipation rate in wall-bounded turbulence. In particular, we would like to examine whether the PDFs outside the buffer layer are independent of the distance from the wall and also of the flow Reynolds number.

In Sec. II, a brief description of the DNS data, the coordinate system, and the PDFs is given. In Sec. III, the velocity PDFs are examined. The PDFs of the first derivatives, the second derivatives, and the pseudodissipation rate are investigated in Secs. IV, V, and VI, respectively. We conclude with a brief summary in Sec. VII.

II. PRELIMINARY CONSIDERATIONS

In our discussions we follow the conventional coordinate system in which x is the streamwise direction, y is the wall normal direction, and z is the spanwise direction. We will also use indices 1, 2, and 3 to denote x, y, and z directions, respectively, and a comma (,) followed by a subscript denotes a derivative with respect to the subscript.

The data used in this study are from temporal DNS of turbulent incompressible channel flow. The flow is taken to be periodic in the streamwise and spanwise directions, both of which are homogeneous directions. The DNS data from four different simulations are used in this study. The sources are Handler,[7] Breuer,[8] the data of Zang used in Dinavahi and Zang,[9] and Kim.[10] The Reynolds numbers based on the channel half-height and the wall friction velocity for these data are 125, 180, 395, and 318, respectively. The rms values of the three velocity components, u,v,w, and that of the velocity derivative $\partial u/\partial x$ are plotted against y^+ in Fig. 1. The quantities in Fig. 1 are normalized by wall quantities. The peak in $u_{\rm rms}$ increases in magnitude with increasing Reynolds number and occurs at the same y^+ ($\approx$15) for all four Reynolds numbers. Similar observations hold for $(\partial u/\partial x)_{\rm rms}$ as well. For $v_{\rm rms}$ and $w_{\rm rms}$, all four curves are clearly separated and the peak value increases with the Reynolds number and shifts to the right.

It is more interesting to look at the ratios of the rms values of the velocity derivatives, which give a measure of

[a)]Presently with SAIC, 134 Holiday Court, Suite 318, Annapolis, Maryland 21108.

 1070-6631/95/7(5)/1122/8/$6.00

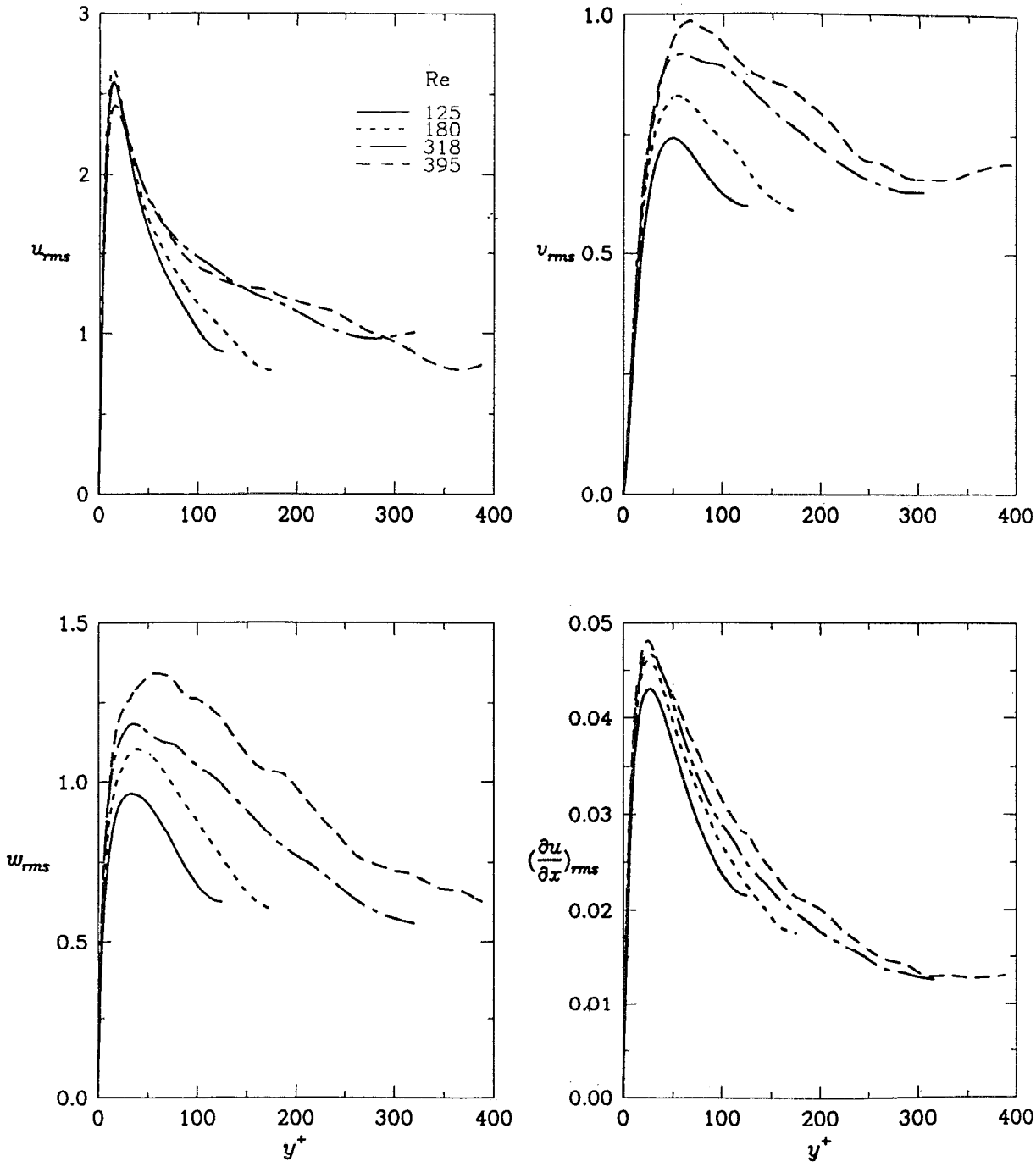

FIG. 1. The rms values of the velocities and the derivative of u.

the local isotropy, rather than the rms values themselves. The ratios $(u_{i,1})_{\rm rms}/(u_{i,2})_{\rm rms}$, $(u_{i,3})_{\rm rms}/(u_{i,2})_{\rm rms}$ for $i=1,2,3$ are shown in Fig. 2. There are two observations to be made from this set of graphs. First, the curves for each of these ratios collapse to a single curve, irrespective of the Reynolds number. Second, each of the six ratios asymptotes to a different number as the channel centerline is approached. We have to keep in mind that the farfield here is the centerline of a channel, unlike the boundary layer of external flow. At the centerline of a channel, the turbulence experiences a set of constraints that are different from those in external flow. The approximate asymptotic values of these ratios are tabulated in Table I.

From each of the datasets, three y^+ locations are selected for PDF calculations. The selected y^+ locations for the Re $=318$ dataset are shown as symbols on a plot of u^+ vs y^+ in Fig. 3, where $u^+=u/u_\tau$, $y^+=yu_\tau/\nu$ and u_τ, and ν are the wall friction velocity and kinematic viscosity, respectively.

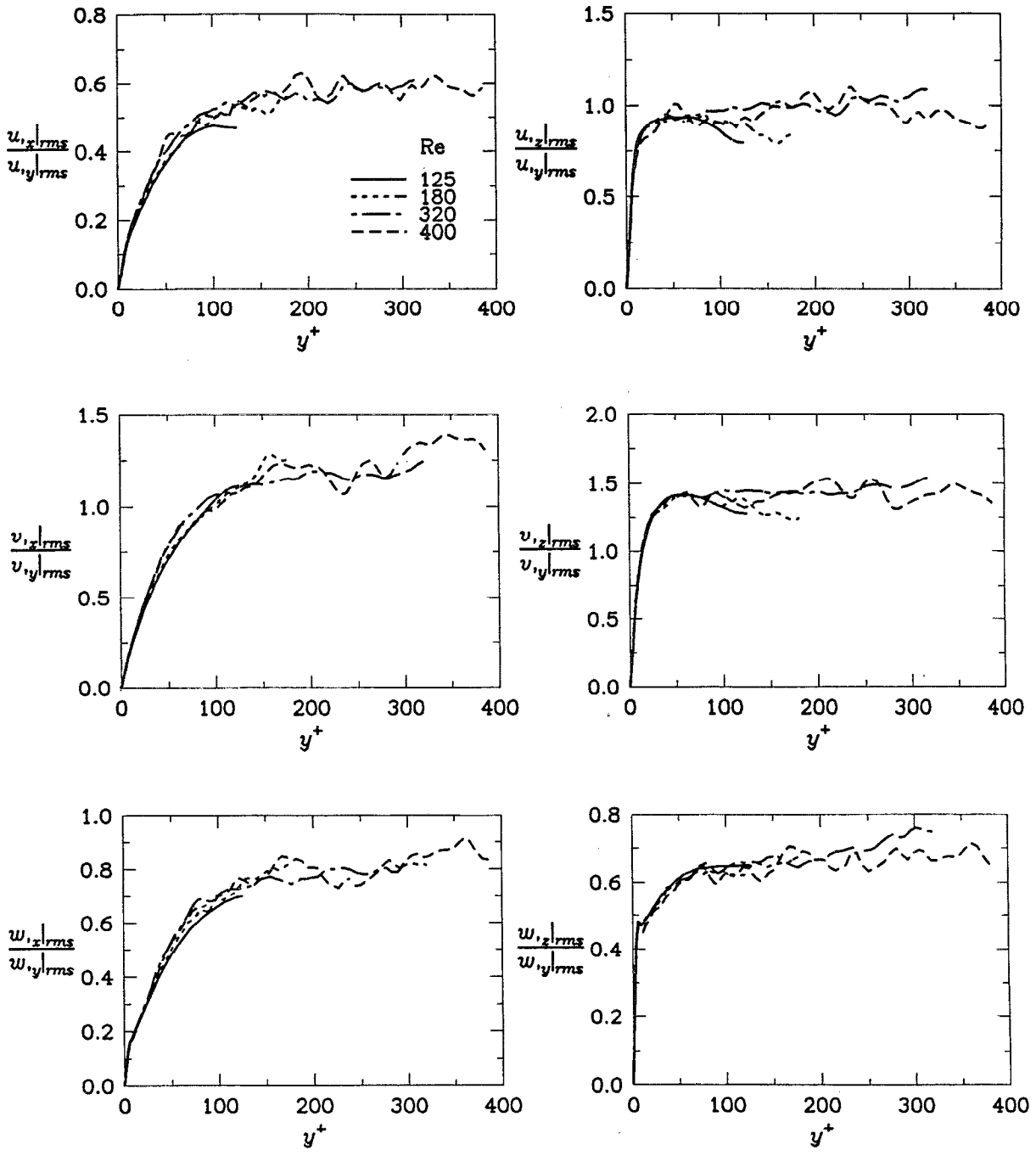

FIG. 2. Ratios of the rms velocity derivatives.

In each case two locations are selected in the log layer and one at the centerline. By symmetry each selected y corresponds to two horizontal planes: one on each side of the channel centerline, thus doubling the number of points.

TABLE I. Asymptotic values of the ratios of the rms velocity derivatives.

$\frac{(u_{,x})_{\rm rms}}{(u_{,y})_{\rm rms}}$	$\frac{(u_{,z})_{\rm rms}}{(u_{,y})_{\rm rms}}$	$\frac{(v_{,x})_{\rm rms}}{(v_{,y})_{\rm rms}}$	$\frac{(v_{,z})_{\rm rms}}{(v_{,y})_{\rm rms}}$	$\frac{(w_{,x})_{\rm rms}}{(w_{,y})_{\rm rms}}$	$\frac{(w_{,z})_{\rm rms}}{(w_{,y})_{\rm rms}}$
0.6	1.0	1.2	1.4	0.8	0.65

Other than this symmetry, we did not make full use of the symmetry group of the channel, Sirovich.[11] The y^+ locations for the other datasets are selected in a similar fashion. The different datasets and the selected y locations are summarized in Table II. The large number of samples used for the first three datasets essentially ensured accurate PDFs. For the fourth Reynolds number, we had access to only one realization, giving us around 9.5 million samples.

In the current simulations, x and z being the homogenous directions, the PDF of a random variable ϕ is only a function of the wall normal direction and the Reynolds num-

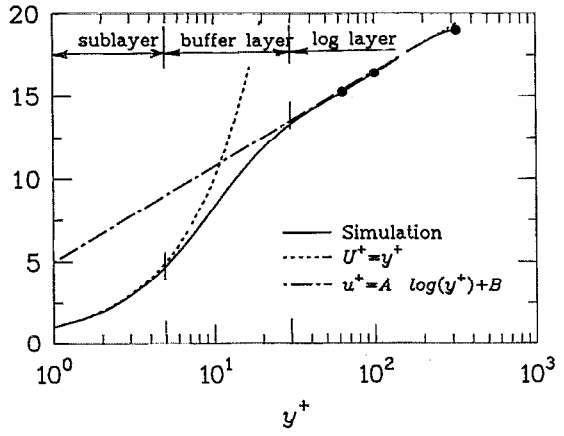

FIG. 3. U^+ vs y^+ for Re=318.

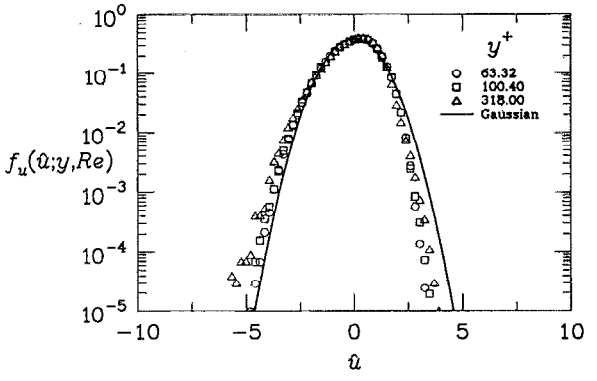

FIG. 4. PDFs of u for Re=318.

ber of the flow; hence, it is reasonable to consider $f_\phi(\hat{\phi};y,\mathrm{Re})$, where

$$\hat{\phi}=\frac{\phi-\langle\phi\rangle}{[\langle(\phi-\langle\phi\rangle)^2\rangle]^{1/2}} \tag{1}$$

is a locally normalized fluctuation from the mean.

III. VELOCITIES

In this section, the PDFs of the fluctuating velocities are examined as a function of the wall normal distance and Reynolds number. In all the PDF plots the Gaussian curve is also shown for comparison. In Fig. 4, the PDFs of the u velocity, $f_u(\hat{u};y,\mathrm{Re}=318)$, at the three selected y locations are plotted. The various PDFs to a good approximation collapse onto a single curve, indicating that the statistics of u are independent of the y location. Similar PDFs for v and w (not shown) are also observed to be independent of the y location.

After establishing the independence of y at each of the four Reynolds numbers for each of the velocity components, we go on to examine the issue of independence with respect to Reynolds number. For this purpose, we use the PDF, $f_u(\hat{u};\mathrm{Re})$, which is obtained by averaging $f_u(\hat{u};y,\mathrm{Re})$ from the three y locations. The PDFs independent of y are constructed similarly for v and w. The PDFs, $f_u(\hat{u};\mathrm{Re})$, $f_v(\hat{v};\mathrm{Re})$, and $f_w(\hat{w};\mathrm{Re})$, at the four Reynolds numbers are plotted in Figs. 5, 6, and 7, respectively. From these figures it is seen that velocity PDFs are relatively independent of the Reynolds number as well. The PDFs of u are negatively skewed and those of v are positively skewed in the tails, whereas the PDFs of w are very close to the Gaussian. This trend is also confirmed by observing the skewness factors presented in the next section in Table III.

IV. FIRST DERIVATIVES OF THE VELOCITIES

In this section, we examine the dependence of the PDFs of the velocity derivatives on the y location and Reynolds number. We will also consider the hypothesis by Narasimha[4] that the PDFs of the first derivatives can be represented by a Gaussian core with exponential tails.

In Fig. 8, PDFs for $u_{,y}$ at three y locations in the log layer are plotted from the data at a Reynolds number of 318. These PDFs agree well with each other up to three standard deviations. The PDF corresponding to the channel centerline is symmetric, and at the other two locations, the PDFs are skewed toward the positive side. Further, it is observed that with increasing y^+, the left leg of the PDF curve gradually moves farther away from the Gaussian toward the PDF at the centerline of the channel. The PDFs of the other eight first derivatives (not shown) are independent of the y location. After establishing the independence of the y location for the first derivatives (except for that of $u_{,y}$), the PDFs for these eight first derivatives are calculated by using the entire dataset from the three y locations. These PDFs can be denoted as $f_{u_{i,j}}(\hat{u}_{i,j};\mathrm{Re})$ $(j\neq 2)$, showing the independence of y, and are plotted in Fig. 9. The PDFs of $u_{,z}$, $v_{,x}$, $v_{,z}$, $w_{,x}$, and $w_{,z}$ are symmetric. The PDFs of the three derivatives that go into the continuity equation—$u_{,x}$, $v_{,y}$, and $w_{,z}$—are skewed toward the negative side in the tails. In order to ascertain that this deviation in the tails is not due to statistical scatter, a sensitivity study was carried out for the Reynolds number

TABLE II. Selected y^+ locations for different Reynolds numbers.

Author	Re	y^+ locations	Grid	Number of realizations	Number of samples
Handler	125.0	50.50, 82.88, 125.00	64 × 49 × 64	80	16 056 320
Breuer	180.0	59.12, 99.07, 180.00	128 × 129 × 128	100	211 353 600
Zang	318.0	63.32, 100.40, 318.00	216 × 163 × 108	20	76 049 280
Kim	395.0	40.74, 102.32, 395.00	256 × 193 × 192	1	9 486 336

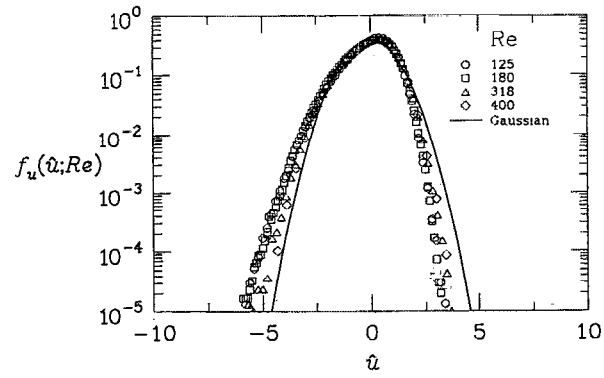

FIG. 5. PDFs of u for the Reynolds numbers shown.

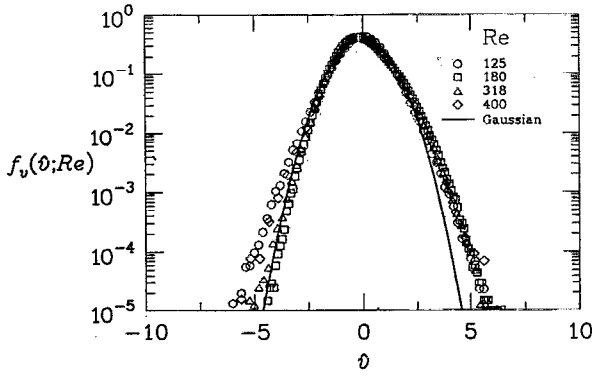

FIG. 6. PDFs of v for the Reynolds numbers shown.

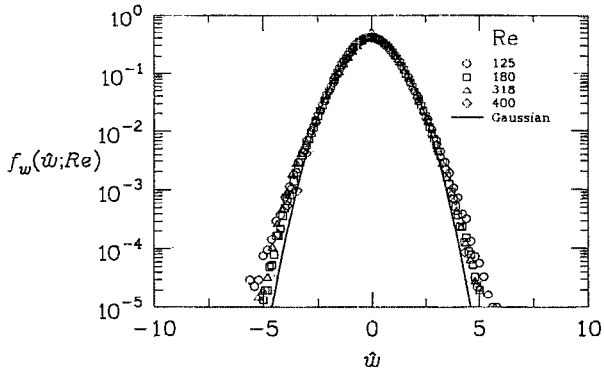

FIG. 7. PDFs of w for the Reynolds numbers shown.

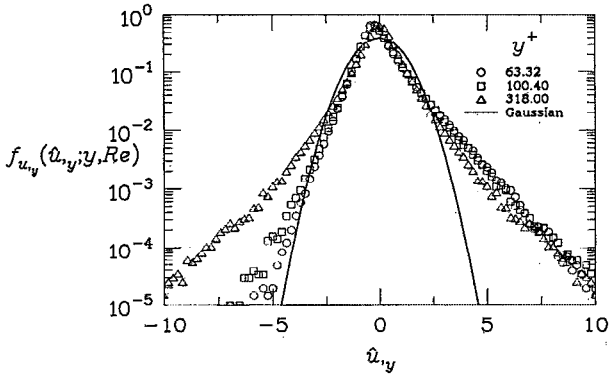

FIG. 8. PDFs of $u_{,y}$ for Re=318.

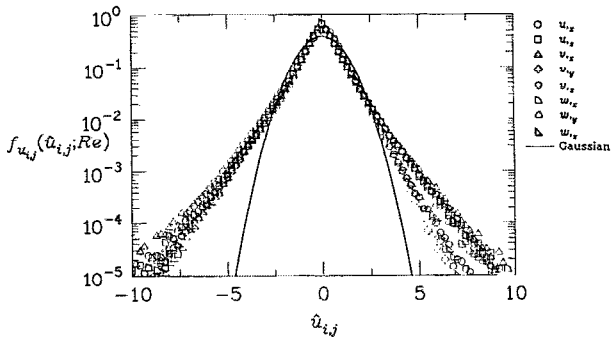

FIG. 9. PDFs of the first derivatives for Re=318.

equal to the 180 case, and it was confirmed that the noted asymmetry was indeed present and not an artifact of statistical scatter.

The flatness and skewness factors for the velocities and their first derivatives (except for $u_{,y}$) for different Reynolds numbers are provided in Tables III and IV. The data in these tables confirm the trends observed visually from the plots. Kuo and Corrsin[2] report that flatness factors of the first and second derivatives increase monotonically with increasing Reynolds numbers, however, with the exception of the flatness factors of $u_{,x}$ and $v_{,x}$ there is no discernible trend for the limited range of Reynolds numbers considered here.

To observe the behavior of the PDFs at different Reynolds numbers, the PDFs of $u_{,x}$ at the four different Reynolds numbers and that from the experiment of Van Atta and Chen[12] are plotted in Fig. 10. The data of Van Atta and Chen are from an atmospheric boundary-layer experiment conducted at sea level. Three observations can be made from this figure. First, all the PDFs, four from the DNS, and one from the experiment agree quite well up to four standard deviations. Second, there is a Reynolds number trend in the tails. The tails are becoming wider with increasing Reynolds number. Finally, there is a slight negative skew in the tails of the PDF of $u_{,x}$.

Similar plots (not shown) were created for the other first derivatives, and it was observed that not only are the PDFs of the first derivatives (except $u_{,y}$) independent of the y location, but also, are independent of Reynolds number.

Narasimha[4] asserts that the PDFs of first derivatives can be approximated by a Gaussian core and exponential tails of the type

$$f(x)=ae^{-x^2/\sigma^2}+be^{-\alpha|x|}. \tag{2}$$

In order to test the above hypothesis, we selected the symmetric PDF $u_{,z}$, since we cannot use a PDF of $u_{,x}$ that is asymmetric. A least squares curve was fit to the above equation (2). The calculated curves and the data for the four Reynolds numbers are plotted in Fig. 11, where the constants used in computing the curve are $a=0.293$, $b=0.293$, $\sigma=0.831$, and $\alpha=1.01$. The Gaussian core with exponential tails seems to be a good fit for symmetric PDFs of the first derivatives of velocity components.

TABLE III. Skewness factors.

Re	u	$u_{,x}$	$u_{,z}$	v	$v_{,x}$	$v_{,y}$	$v_{,z}$	w	$w_{,x}$	$w_{,y}$	$w_{,z}$
125	−0.68	−0.34	0.00	−0.01	0.01	−0.49	−0.01	0.00	−0.02	−0.01	−0.26
180	−0.36	0.06	−0.05	0.41	−0.16	−0.43	0.02	−0.03	0.00	0.07	−0.32
320	−0.45	−0.62	−0.09	0.31	−0.06	−0.38	−0.05	−0.04	−0.03	−0.01	−0.36
400	−0.41	−0.85	0.13	0.19	0.06	−0.33	−0.03	0.06	0.09	−0.01	0.32

V. SECOND DERIVATIVES OF THE VELOCITIES

We now turn our attention toward the second derivatives of the fluctuating quantities. In Fig. 12 the PDFs, $f_{u_{,xx}}(\hat{u}_{,xx};y,\mathrm{Re}=318)$, are plotted. It can be seen that all three PDFs fall on the same curve, indicating that the PDFs outside the buffer layer are independent of the y location. Similar behavior is observed for the other second derivative PDFs as well. Therefore, a single PDF, $f_{u_{,xx}}(\hat{u}_{,xx};\mathrm{Re}=318)$ can be calculated by using the data from all of these locations for each of the second derivatives. In Fig. 13, the PDFs of all the 18 s derivatives $f_{u_{i,jk}}(\hat{u}_{i,jk};\mathrm{Re}=318)$ are plotted. These PDFs are very close to each other up to about four standard deviations, and beyond that, there is some spread in the tails.

These observations are verified again using the data at the other three Reynolds numbers. A single curve for the PDF of $u_{,xx}$ was calculated using the data at the different y locations outside the buffer layer at each of the Reynolds number. To test the hypothesis of Reynolds number independence, these four curves are plotted in Fig. 14. It can be seen that the four curves agree quite well for up to four standard deviations, but there is some spread in the tails. There is a Reynolds number trend in the tails—the PDFs of higher Reynolds number data have wider tails.

VI. DISSIPATION RATE

In this section, we examine what is sometimes called the "pseudodissipation rate," defined as

$$\phi=\frac{1}{\mathrm{Re}}(u_{i,j}u_{i,j}) \quad (i,j=1,2,3), \tag{3}$$

where repeated indices imply summation and the overbar denotes Reynolds averaging. We would like to point out that in the turbulence modeling literature, cf. Speziale,[13] the mean, $\bar{\phi}$ is referred to as the kinetic energy dissipation rate and modeled as such, even though it is not the true dissipation rate, and this is one of the reasons for looking at this quantity. In Fig. 15 the PDFs of $\log(\phi)$ at different Reynolds numbers are plotted. On the same plot the Gaussian (normal) PDF is plotted for comparison. This clearly demonstrates that at the two Reynolds numbers considered, the pseudodissipation rate is lognormal outside the buffer region. The lognormality of this quantity for isotropic turbulence is verified by Yeung and Pope.[14] However, in the sublayer and the buffer region, the PDF (not shown) of $\log(\phi)$ is skewed to the left.

The PDF for $\log(\phi)$ is substantially different from the exponential distributions, which we have obtained for the PDFs of the individual derivative, $u_{i,j}$. The PDF of $\log(\phi)$ falls off far more gently. This might give the appearance of an incompatibility. We briefly indicate that no conflict is present in these very different PDFs. Toward this end we define $P = P(\widehat{u_{i,j}})$ to be the PDF in the nine derivatives contained in $u_{i,j}$. Thus,

$$\int P(\widehat{u_{i,j}})\,d\widehat{u_{i,j}}=1, \tag{4}$$

where $d\widehat{u_{i,j}} = \Pi_{i,j=1}^{3}\widehat{u_{i,j}}$ is the element of volume in the nine-dimensional $\widehat{u_{i,j}}$ space. All reduced PDFs are determined by $P(\widehat{u_{i,j}})$, e.g., $P_1(\widehat{u_{\alpha,\beta}})$, the one-dimensional PDF in $\widehat{u_{\alpha,\beta}}$ is given by

$$\int P(\widehat{u_{i,j}})\frac{d\widehat{u_{i,j}}}{d\widehat{u_{\alpha,\beta}}}=P_1(\widehat{u_{\alpha,\beta}}). \tag{5}$$

Similarly, if $\epsilon=|\widehat{u_{i,j}}|$ and Ω denote spherical coordinates in $\widehat{u_{i,j}}$ space, then the one-dimensional PDF in ϵ is given by

$$P_1(\epsilon)=\int P(\widehat{u_{i,j}})\,d\Omega. \tag{6}$$

The relation between $P_1(\epsilon)$ and $P_1(\epsilon^2)$ is simply $P_1(\epsilon)=2\epsilon P_1(\epsilon^2)$. In order to see the compatibility of the two types of PDFs under discussion, it is convenient to think in terms of discrete probabilities. Thus, if $\widehat{u_{i,j}}$ space is discretized in each of the nine directions into, say, N slices, there are N^9 values for $P(\widehat{u_{i,j}})$. Equation (6) with $P_1(\epsilon)$ represents N relations in these N^9 quantities, as does (5), with $P_1(\widehat{u_{\alpha,\beta}})$ given. Thus, there are $10N$ relations in the N^9 relations that shows how underdetermined the conditions are with $P_1(\widehat{\ln\phi})$ and $P_1(\widehat{u_{\alpha,\beta}})$ both prescribed. Clearly, the results shown in Figs. 9 and 15 can be regarded as one solution to this vastly underdetermined problem.

TABLE IV. Flatness factors.

Re	u	$u_{,x}$	$u_{,z}$	v	$v_{,x}$	$v_{,y}$	$v_{,z}$	w	$w_{,x}$	$w_{,y}$	$w_{,z}$
125	3.57	5.12	6.33	3.75	5.57	5.34	6.70	3.61	4.70	6.53	4.89
180	3.73	6.29	7.59	3.72	7.66	5.40	7.41	3.28	5.89	7.14	5.54
320	3.17	6.80	7.48	3.49	8.99	5.49	7.08	3.41	7.54	7.00	5.75
400	3.09	8.56	6.99	3.77	10.54	5.73	8.08	3.24	7.48	6.07	5.41

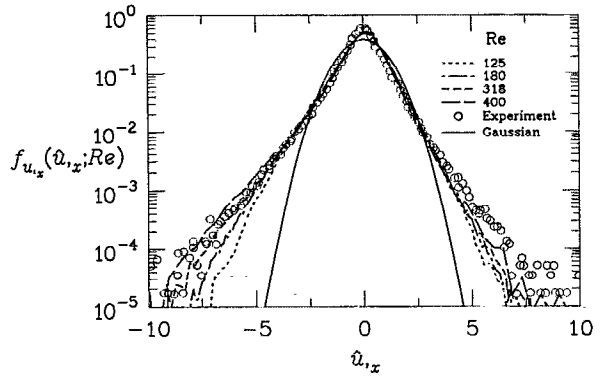

FIG. 10. Comparison of PDFs of $u_{,x}$ calculated from DNS data with those from the experiments of Van Atta and Chen.

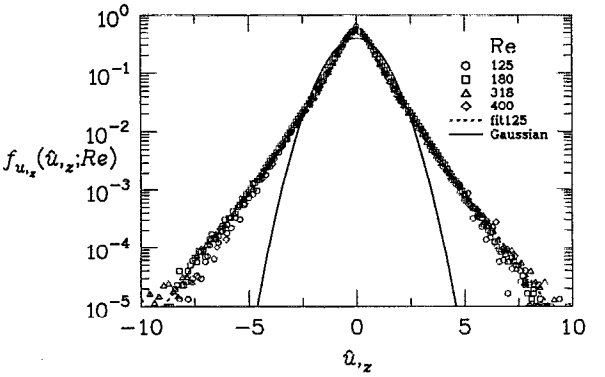

FIG. 11. Least squares fit for the PDFs of $u_{,z}$.

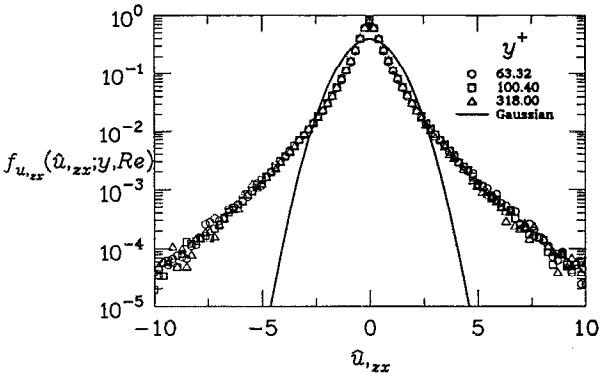

FIG. 12. PDFs of $u_{,zz}$ for Re=318.

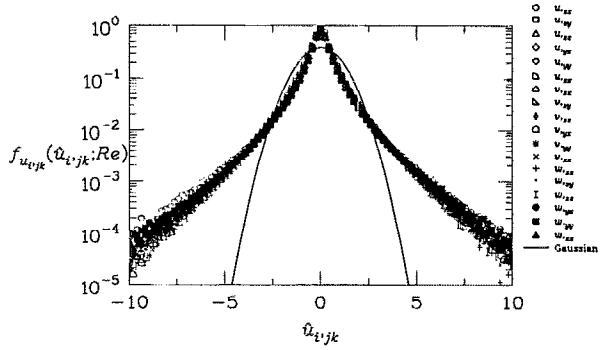

FIG. 13. PDFs of the second derivatives for Re=318.

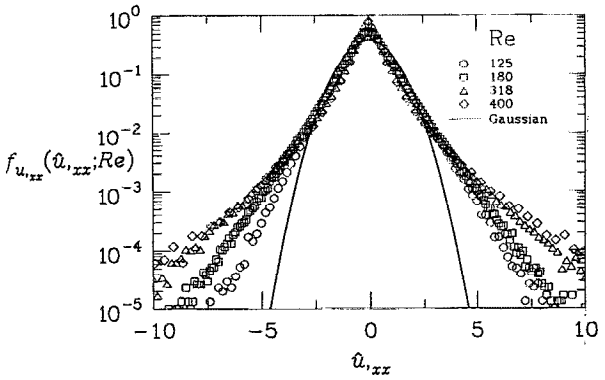

FIG. 14. PDFs of $u_{,xx}$ for the Reynolds numbers shown.

VII. CONCLUDING REMARKS

By analyzing the data at the four Reynolds numbers (125, 180, 318, and 395), it is concluded that the PDFs of the fluctuating quantities are independent of the y location when outside the buffer layer, and that they are also independent of the Reynolds number of the flow. The PDFs of u have a small negative skew in the tails. The PDFs of v are positively skewed in the tails and PDFs of w are symmetric and appear to be close to Gaussian.

The ratios of the rms values of the velocity derivatives are independent of Reynolds number and attain asymptotic values away from the wall. The PDFs of the first derivatives (except for that of $u_{,y}$) are independent of y for locations outside the buffer layer. Not only are the symmetric PDFs independent of y, but they also appear to have the same universal shape, irrespective of the particular quantity and the Reynolds number: the shape of a Gaussian core and exponential tails.

The PDFs of all the second derivatives are also independent of the y location. The lognormality of the pseudodissipation rate for y location outside the viscous sublayer is also verified.

The appearance of universal PDFs was reported earlier for the case of Rayleigh–Bénard convection.[5] As stated there: "The mechanism that is responsible for the tendency toward universality is not obvious." As is seen in Figs. 1 and

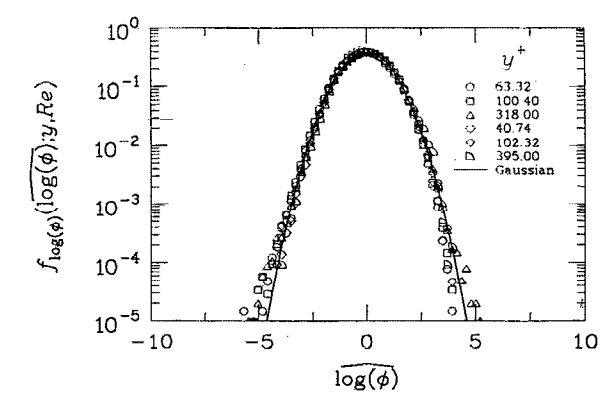

FIG. 15. PDFs of the pseudodissipation rate, ϕ.

2, there is a strong variation in the various rms values as we move across the channel. Nevertheless, a substantial degree of universality in the PDFs still results. To some extent the choice of the variable, $\hat{\phi}$, see Eq. (1), forces some uniformity. This transformation removes local conditions to the extent that $\hat{\phi}$ has a zero mean and unit variance. To further investigate the basis of universality, we remark that on dimensional grounds we know that $f_\phi = f_\phi(\hat{\phi}; y^+, \mathrm{Re})$. For the data under consideration, it would appear that for $\mathrm{Re} > 125$ we are in the asymptotic range, i.e., the Re number dependence can be ignored. Furthermore, when in the scaling region, $1 \ll y^+ \ll \mathrm{Re}$, standard arguments suggest that y^+ will cancel out in $\hat{\phi}$. However, this does not explain why the PDF in the core region, $y \sim \mathrm{Re}$, are well fit by the same PDF, e.g., see Figs. 4 and 12. On the other hand, this is not true, except for the first two log units of the PDF for $(\partial u/\partial y)$, Fig. 8. In this case symmetry requires that the PDF be an even function in the variable at the centerline of the channel, which the figure confirms. But, elsewhere we expect to find skewed PDFs and the figure also shows this to be the case. The fact that there are such departures from universality implies that no simple theory will explain the universality, which has been found.

Finally, we remark that the universality found in the PDFs for second (and doubtless higher) derivatives might have been anticipated on the grounds that successively higher derivatives emphasize successively smaller scales, which might be expected to have more universal features.

ACKNOWLEDGMENTS

We thank Dr. Handler, Dr. Kim, and Dr. Zang for providing us the data at the Reynolds numbers of 125, 395, and 318, respectively. The work of Dinavahi was supported by the Theoretical Flow Physics Branch of the NASA Langley Research Center under NASA Contract No. NAS1-18599. The authors thank Dr. Akiva Yaglom for his constructive comments on this paper. Kenny Breuer's time was supported by a grant from ONR No. N00014-92-J-1918 monitored by Pat Purtell. L. Sirovich was supported by Grant No. NSF IRI-911645.

[1] G. K. Batchelor and A. A. Townsend, "The nature of turbulent motion at large wavenumbers," Proc. R. Soc. London Ser. A **199**, 238 (1949).
[2] A. Y.-S. Kuo and S. Corrsin, "Experiments on internal intermittency and fine-structure distribution in fully turbulent fluid," J. Fluid Mech. **50**, 285 (1971).
[3] Z.-S. She, E. Jackson, and S. A. Orszag, "Scale-dependent intermittency and coherence," J. Sci. Comput. **3**, 407 (1988).
[4] R. Narasimha, "The utility and drawbacks of traditional approaches," in *Whither Turbulence?*, edited by J. L. Lumley (Springer-Verlag, New York, 1989), pp. 26–28.
[5] S. Balachandar and L. Sirovich, "Probability distribution functions in turbulent convection," Phys. Fluids A **3**, 919 (1991).
[6] S. P. G. Dinavahi, "Probability density functions in turbulent channel flow," NASA CR 4454, 1992.
[7] R. A. Handler, E. W. Hendricks, and R. I. Leighton, "Low Reynolds number calculation of turbulent channel flow: A general discussion," NRL Memorandum Report No. 6410, February, 1989.
[8] K. S. Breuer, Department of Aeronautics and Astronautics, Report No. CFDL TR-91-5, Massachusetts Institute of Technology, 1991.
[9] S. P. G. Dinavahi and T. A. Zang, "Reynolds stress budget in a transitional channel flow," *Instability, Transition, and Turbulence* (Springer-Verlag, New York, 1992), p. 327.
[10] J. Kim, "On the structure of pressure fluctuations in simulated turbulent channel flow," NASA TM 101084, 1989.
[11] L. Sirovich, "Turbulence and the dynamics of coherent structures," parts I, II, and III, Q. Appl. Math. **XLV**, 561 (1982).
[12] C. W. Van Atta and W. Y. Chen, "Structure functions of turbulence in the atmospheric boundary layer over the ocean," J. Fluid Mech. **44**, 145 (1970).
[13] C. G. Speziale, "Analytical methods for the development of Reynolds-stress closures in turbulence," Annu. Rev. Fluid Mech. **23**, 107 (1991).
[14] P. K. Yeung and S. B. Pope, "Lagrangian statistics from direct numerical simulations of isotropic turbulence," J. Fluid Mech. **207**, 531 (1989).